Available online at www.sciencedirect.com
ScienceDirect
www.elsevier.com/locate/jes
JOURNAL OF ENVIRONMENTAL SCIENCES
www.jesc.ac.cn

Research Article

Reduced rainfall over the Amazon basin in an idealized CO_2 removal scenario: Remote dynamic processes

Q1 *Suqin Zhang*[1,4], *Xia Qu*[1,3,*], *Gang Huang*[1,2,4,*], *Peng Hu*[5,6]

[1] *State Key Laboratory of Numerical Modeling for Atmospheric Sciences and Geophysical Fluid Dynamics, Institute of Atmospheric Physics, Chinese Academy of Sciences, Beijing 100029, PR China*
[2] *Laboratory for Regional Oceanography and Numerical Modeling, Qingdao National Laboratory for Marine Science and Technology, Qingdao 266237, PR China*
[3] *Center for Monsoon System Research, Institute of Atmospheric Physics, Chinese Academy of Sciences, Beijing 100029, PR China*
[4] *University of Chinese Academy of Sciences, Beijing 100049, PR China*
[5] *Yunnan Key Laboratory of Meteorological Disasters and Climate Resources in the Greater Mekong Subregion, Yunnan University, Kunming 650091, PR China*
[6] *Department of Atmospheric Sciences, Yunnan University, Kunming 650500, PR China*

ARTICLE INFO

Article history:
Received 24 January 2024
Revised 21 May 2024
Accepted 21 May 2024
Available online xxx

Keywords:
CO_2 removal
Amazon basin rainfall
El Niño-like warming
Stationary Rossby wave train

ABSTRACT

The Amazon basin plays a crucial role in biodiversity and carbon storage, but its local rainfall is anticipated to decrease under global warming. Carbon dioxide removal (CDR) is being considered as a method to mitigate the impact of global warming. However, the specific effects of CDR on Amazon rainfall have not been well understood. Here, an idealized CDR experiment reveals that the reduced rainfall over the Amazon basin does not recover. Significantly weaker rainfall was found during the ramp-down period compared to the ramp-up period at the same CO_2 concentration. This response is associated with the enhanced El Niño-like warming in the tropical Pacific Ocean during the CDR period. This warming pattern has dual effects: weakening the zonal circulation and causing anomalous descent directly over the Amazon basin, while also triggering a stationary Rossby wave train that propagated downstream and generated anomalous ascent over the Sargasso Sea. This anomalous ascent induces anomalous descent and weakens moisture transport over the Amazon basin by the local meridional circulation. Consequently, precipitation is reduced over the Amazon basin in response to the weakened zonal and meridional circulation. Our findings indicate that even if the atmospheric CO_2 concentration is lowered, the Amazon basin will remain susceptible to drought. Effective local climate adaptation strategies are urgently needed to address the vulnerability of this critical ecosystem.

* Corresponding authors at: State Key Laboratory of Numerical Modeling for Atmospheric Sciences and Geophysical Fluid Dynamics, Institute of Atmospheric Physics, Chinese Academy of Sciences, Beijing 100029, PR China.
Q2 *E-mails:* quxia@mail.iap.ac.cn (X. Qu), hg@mail.iap.ac.cn (G. Huang).

https://doi.org/10.1016/j.jes.2024.05.035
1001-0742

Introduction

The Amazon basin, Earth's largest river basin spanning around 6 million km^2, is a vital hydrological system teeming with rivers, wetlands, and floodplains (Fassoni-Andrade et al., 2021; Towner et al., 2020). Beyond impacting the seven countries it crosses (e.g., Brazil and Peru), the Amazon basin is a key hub of tropical convection, shaping global atmospheric circulation and influencing the carbon, energy, and hydrological cycles (Fassoni-Andrade et al., 2021; Towner et al., 2020). For instance, the Amazon River's main stem annually discharges 2.1×10^5 m^3/s, contributing 20 % of the total global freshwater flow into oceans (Fassoni-Andrade et al., 2021; Towner et al., 2020). This substantial river discharge results from abundant rainfall, averaging 2000–2200 mm per year, mainly sourced from local evapotranspiration and moisture transport from the tropical Atlantic Ocean (Cai et al., 2020; Ciemer et al., 2020; Towner et al., 2020). This rainfall is critical for the local rainforest, biodiversity, and acts as a driving force for atmospheric general circulation (Burleyson et al., 2016; Cai et al., 2020; Fassoni-Andrade et al., 2021; Tang et al., 2016; Towner et al., 2020). A precipitation deficit can reduce ecosystem respiration (Doughty et al., 2015; Thakur et al., 2018) and lead to tree mortality due to hydraulic failure (Bréda et al., 2006), carbon starvation (McDowell et al., 2008), and an increased incidence of wildfires. Consequently, this reduction in biodiversity and the weakened forest-rainfall feedback can promote further drought occurrences (Staal et al., 2020a; Zemp et al., 2017). Additionally, diminished vegetation undermines the rainforest's capacity to absorb carbon, thereby exacerbating global warming and affecting the global climate. For instance, due to increased tree mortality, the Amazon temporarily turned into a carbon source during two major droughts in 2005 and 2010 (Boulton et al., 2022; Feldpausch et al., 2016).

Given the pivotal role of Amazon rainfall, extensive efforts have focused on investigating the multiscale factors influencing it. On the synoptic scale, equatorial Kelvin waves, primarily originating from the Pacific and South America, are recognized as the dominant mode of variability (Liebmann et al., 2009; Mayta et al., 2021). The intraseasonal variability is modulated by equatorial Rossby wave-like disturbances (Mayta and Adames, 2023; Mayta et al., 2022) and the Madden-Julian Oscillation (Liu et al., 2020; Mayta et al., 2020; Reboita et al., 2021). On the interannual timescale, sea surface temperature (SST) anomalies in the Pacific and Atlantic Oceans play a crucial role in influencing Amazon rainfall. Specifically, the warm phase of the El Niño-Southern Oscillation (ENSO) is expected to cause rainfall deficits and drought over the Amazon basin, mainly by modulating the Walker circulation (Cai et al., 2020; Kay et al., 2022; Towner et al., 2020). The tropical Atlantic Ocean affects the rainfall over the Amazon by influencing the location of the Intertropical Convergence Zone (ITCZ), which generally follows the location of the warm SST (Ciemer et al., 2020; Towner et al., 2020; Yoon and Zeng, 2010). Additionally, longer-term factors such as the Pacific Decadal Oscillation and Atlantic Multidecadal Oscillation contribute to Amazon rainfall variability (Cai et al., 2020; Reboita et al., 2021; Towner et al., 2020). Human activities, especially deforestation it causes, also significantly influence rainfall in the Amazon basin. Deforestation, which involves converting forests into pastures and croplands, can directly modify local rainfall patterns. This is due to changes in the moisture cycle and energy balance, which are associated with reduced evapotranspiration and surface roughness, and increased albedo (Li et al., 2022). On broader spatial scales, diminished evapotranspiration could impair the moisture recycling process that transports water vapor from oceans to tropical forests (Baidya et al., 2002; Leite-Filho et al., 2021). Conversely, on smaller scales, deforestation may lead to a patchy distribution of surface roughness and atmospheric heating, potentially increasing rainfall in deforested regions and areas downwind of these patches (Khanna et al., 2018; McGuffie et al., 1995). Most models project an increase in Amazon temperature, at least 0.5 °C higher than the global mean (Torres et al., 2021), but a decrease in Amazon rainfall under the global warming scenario (Almazroui et al., 2021; Cai et al., 2020; Pascale et al., 2019; Thome Sena and Magnusdottir, 2020). Global warming tends to reduce forest viability via increasing dry-season length (Adams et al., 2017; Fu et al., 2013), the frequency of drought and wildfire (Boulton et al., 2022; Brando et al., 2020, Wang and Huang, 2022). Forest degradation can reduce evapotranspiration and hence the moisture transported further westward, reducing rainfall in Amazon basin (Boulton et al., 2022; Salati et al., 1979). And these changes can be further amplified by a large-scale moisture recycling feedback, with increased drought in the Amazon basin (Boulton et al., 2022). Meanwhile, increased El Niño events in the future may also cause a precipitation deficit in the Amazon basin through atmospheric teleconnection (Kay et al., 2022; McGregor et al., 2022).

The previously mentioned studies on Amazon rainfall are mainly focused on modern climatic conditions and global warming scenarios. However, to reduce and prevent dangerous climate change and impacts, a global temperature rise threshold of 1.5 °C/2 °C for the end of 21st century has been set, known as "the Paris Agreement". Achieving this threshold involves various anthropogenic CO_2 removal (CDR) methods, leading to lower atmospheric CO_2 concentrations (IPCC, 2021; Keller et al., 2018). Typically, an idealized CDR scenario is prescribed by the Carbon Dioxide Removal Model Intercomparison Project (CDRMIP), in which the atmospheric CO_2 concentration rises at a rate of 1 % per year until it quadruples, followed by a symmetric decline (Keller et al., 2018). This CDR scenario has been extensively studied, examining temperature, precipitation, carbon cycle, ITCZ, sea level, and more (Cao et al., 2023; Kim et al., 2022; Kug et al., 2022; Park and Kug, 2022; Wu et al., 2015). Upon the recovery of atmospheric CO_2 concentration to pre-industrial revolution levels, the global mean temperature is abnormally high (Qu and Huang, 2023; Wu et al., 2010), impacting water vapor capacity and global mean rainfall. However, the response to CDR varies markedly from region to region, for example, East Asia (Song et al., 2022), South Asia (Zhang et al., 2023), Pacific ITCZ (Zhou et al., 2022), and ENSO (Liu et al., 2023). The evolutionary characteristics and response mechanisms of rainfall over the Amazon basin under such an idealized CDR scenario forms the focus of our investigation.

Please cite this article as: Suqin Zhang, Xia Qu, Gang Huang et al., Reduced rainfall over the Amazon basin in an idealized CO2 removal scenario: Remote dynamic processes, Journal of Environmental Sciences, https://doi.org/10.1016/j.jes.2024.05.035

Table 1 – The detailed information of CMIP6 models used in this study.

No.	Model name	Country	Var label	Horizontal gird	References
1	ACCESS-ESM1-5	Australia	r1i1p1f1	145 × 192	Ziehn et al., 2020
2	CAS-ESM2-0	China	r1i1p1f1	128 × 256	Zhang et al., 2020
3	CanESM5	Canada	r1i1p2f1	64 × 128	Swart et al., 2019
4	CESM2	USA	r1i1p1f1	192 × 288	Danabasoglu et al., 2020
5	CNRM-ESM2-1	France	r1i1p1f2	128 × 256	Séférian et al., 2019
6	GFDL-ESM4	USA	r1i1p1f1	180 × 288	Dunne et al., 2020
7	MIROC-ES2L	Japan	r1i1p1f2	64 × 128	Hajima et al., 2020
8	NorESM2-LM	Norway	r1i1p1f1	96 × 144	Seland et al., 2020
9	UKESM1-0-LL	UK	r1i1p1f2	144 × 192	Senior et al., 2020

1. Data and methods

The study leverages several experiments from the Coupled Model Intercomparison Project six (CMIP6), including: (1) historical experiment, in which the models are compelled by observed atmospheric CO_2 concentration from the mid-nineteenth century to 2014 (Eyring et al., 2016); (2) pre-industrial control (piControl) experiment, in which the atmospheric CO_2 concentration and the climate system conditions were held at pre-industrial level (Eyring et al., 2016), serves as a reference for the 1 %CO2 experiment; (3) 1pctCO2 experiment. The same as the piControl experiment, except that the atmospheric CO_2 concentration increased by 1 % per year until it quadrupled (Eyring et al., 2016); and (4) 1pctCO2-cdr experiment, starting from the climate states in the 140th year of the 1pctCO2 experiment, CO_2 concentration drops at a rate of 1 % per year for 140 years to recover to the pre-industrial level, and then stays constant for 60-year restoring period (Keller et al., 2018). The combined 1pctCO2 and 1pctCO2-cdr experiments form the idealized CDR scenario, spanning 280 years. This scenario, marked by substantial CO_2 concentration changes, aims for a high signal-to-noise ratio. The response of the climate system under the idealized CDR scenario is assessed relative to the climatology of the last 100 years of piControl experiments. Monthly outputs from nine models participating in these experiments, detailed in Table 1, are employed. Each model contributes a single run for analysis. The Multi-Model Ensemble Mean (MME) approach is employed to reduce internal variability and systematic biases. The response is deemed robust when the signs of results from more than six models align with that of the MME. This study primarily concentrates on the austral summer (DJF) mean, a period when the majority of the annual total rainfall occurs (Cai et al., 2020; Fassoni-Andrade et al., 2021).

To evaluate the simulation performance of CMIP6 models, this study employs the monthly mean reanalysis and observational datasets, which include: (1) Global Precipitation Climatology Project (GPCP) monthly precipitation dataset with a horizontal resolution of 2.5° × 2.5° (Adler et al., 2018); (2) National Centers for Environmental Prediction-Department of Energy (NCEP-DOE) reanalysis data with a horizontal resolution of 2.5° × 2.5° (Kanamitsu et al., 2002); (3) Hadley Centre Global Sea Ice and Sea Surface Temperature (HadISST) data with a horizontal resolution of 1.0° × 1.0° (Rayner et al., 2003). The climatology of DJF mean in 1979–2014 represents the current climate of the Amazon basin, which is compared with that of historical experiments to assess the performance of CMIP6 models. All above CMIP6 and reanalysis datasets are spatially interpolated into a common 1° × 1° grid by a bilinear interpolation.

2. Results

2.1. *Present-day climate of the Amazon basin and model simulations*

The Amazon basin, nestled within the South American monsoon zone, experiences robust convection during the austral summer with pronounced upwelling (Fig. 1a and b; Marengo et al., 2012). The precipitation pattern, shaped by the South Atlantic Convergence Zone (SACZ), displays a distinctive northwest-southeast orientation, defining the primary system of the South American monsoon (Llopart et al., 2020). Trade winds facilitate a north-easterly or easterly moisture flow from the tropical Atlantic Ocean to the Amazon basin, generating a potent moisture flux convergence (Fig. 1b and c) pivotal for sustaining an active SACZ (Durán-Quesada et al., 2012; Muñoz et al., 2015). The CMIP6 MME simulations reasonably reproduce the above rainfall-related distributional features, but with some slight difference in magnitude. Compared to the observations, the CMIP6 MME simulations are weaker in terms of rainfall, and rainfall-related variables (e.g., vertical velocity). For the underlying driver, sea surface temperature (SST), the CMIP6 models have double ITCZ bias (Fig. 1e and f), accompanied by a positive rainfall bias in the southeast Pacific (Fig. 1b). This recurring double ITCZ bias, observed from CMIP3 to CMIP6 model simulations, remains a focal point in climate modeling research (Adam et al., 2018; Si et al., 2021).

The Taylor diagram systematically evaluates the model performance skill across the domain (45°S-45°N, 180°−30°W) for rainfall and related variables (Fig. 2). Spatial correlation coefficients between the simulation of individual models and observations consistently surpass 0.6, except for the vertical velocity at 500 hPa in CAS-ESM2–0 model. The simulation performance of CMIP6 MME for all variables outperforming any single model, with the minimum correlation coefficient higher than 0.79. We therefore utilize the CMIP6 MME to scrutinize the response of Amazon basin rainfall under the idealized CDR scenario.

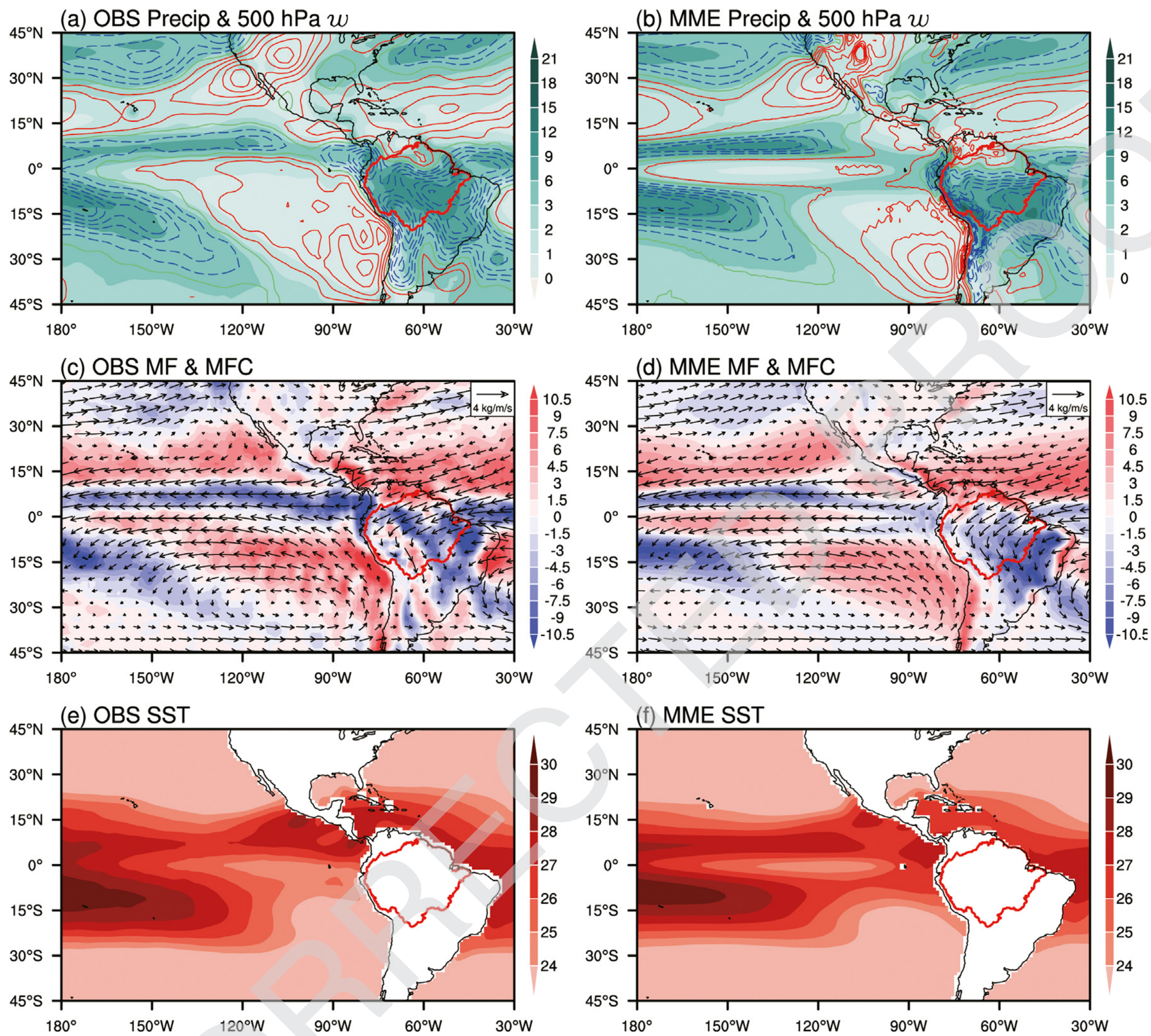

Fig. 1 – Climatology (a and b) precipitation (shading; unit: mm/day) and 500 hPa vertical velocity (contour; unit: 10^{-2} Pa/s), (c, d) vertically integrated moisture fluxes from the surface to 100 hPa (vector; unit: 10^2 kg/(m•s)) and their divergence (shading; unit: 10^{-5} kg/(m^2•s)), and (e, f) SST (shading, unit: °C) of DJF mean climate variables in 1979–2014. Left panel: NCEP-DOE reanalysis or HadISST results; Right panel: CMIP6 MME results. The red solid line denotes the Amazon basin (https://github.com/gamamo/AmazonBasinLimits/tree/master).

2.2. *Irreversible response of austral summer rainfall over the Amazon basin*

Fig. 3a shows the evolution of anomalous DJF mean rainfall over the Amazon basin under the idealized CDR scenario. Along with the increase in CO_2 concentration, the Amazon basin experienced a notable decline in rainfall, surpassing 15 %, leading to an abnormally dry situation (red curve). Here, two 40-year periods for the initial and peak levels of CO_2 concentration are chosen, i.e., Years 1–40 (RU) and Years 101–140 (Peak). Precipitation decreased significantly in the Amazon basin during the CO_2 peak compared to the RU phase, and the result passes the inter-model sign agreement test and the significance test of 90 % difference in mean (Fig. 3b and Appendix A Fig. S1). This feature aligns with the results under the global warming scenario (Almazroui et al., 2021; Thome Sena; Magnusdottir 2020). Subsequently, as CO_2 concentration decreases, rainfall begins to increases (blue curve). However, the recovery is slower than the initial decline, resulting in a significant and robust reduction in precipitation in the Amazon basin during the RD (Years 241–280) period compared to the RU (Years 1–40) period with the same averaged CO_2 concentration (Fig. 4c and Appendix A Fig. S1). Among the nine modes analyzed, eight models exhibit anomalous drought condition in Amazon basin, with the exception for the MIROC-ESM2L model (Appendix A Fig. S2). This suggests that the asymmetric response of Amazon basin rainfall is robust. Eventually, Amazon rainfall has not fully recovered and remains below the initial level after the 60-year CO_2 resotring period (Fig. 3a). Besides, reduced rainfall also appears over the equatorial North Pacific and Atlantic, while enhanced rainfall occurs over the equatorial South Pacific, indicating a southward displacement of the ITCZ reported in previous studies (Kug et al., 2022). Notably, increased rainfall is also noted over the Florida Peninsula and the Sargasso Sea.

Please cite this article as: Suqin Zhang, Xia Qu, Gang Huang et al., Reduced rainfall over the Amazon basin in an idealized CO2 removal scenario: Remote dynamic processes, Journal of Environmental Sciences, https://doi.org/10.1016/j.jes.2024.05.035

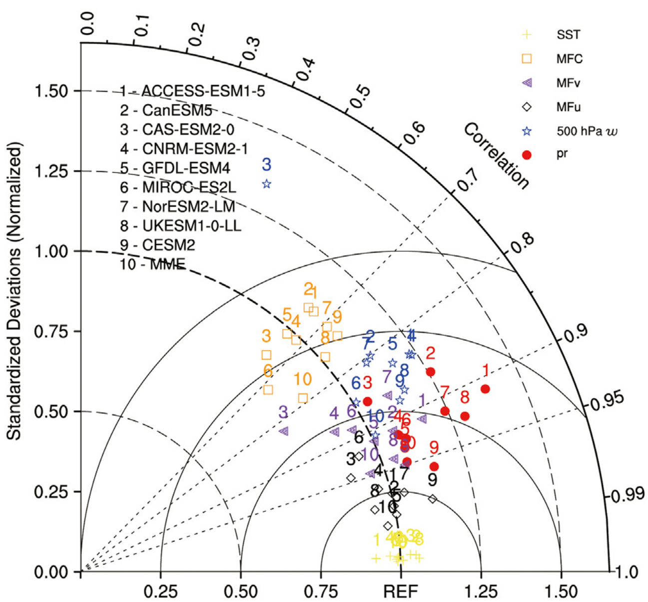

Fig. 2 – Taylor diagram of climatological variables in 1979–2014. The reference point is the results of NCEP-DOE reanalysis or HadISST data. Numbers 1–9 represent the model serial numbers, and number 10 denotes the result of CMIP6 MME.

To comprehend this asymmetric response of rainfall over the Amazon basin, moisture budget analysis is employed (Qu et al., 2015; Zuo et al., 2019) as expressed by Eq. (1):

$$P' = E' - \langle \vec{V}' \cdot \nabla_h \bar{q} \rangle - \langle \bar{\vec{V}} \cdot \nabla_h q' \rangle - \langle \vec{V}' \cdot \nabla_h q' \rangle - \langle \omega' \cdot \partial_p \bar{q} \rangle - \langle \bar{\omega} \cdot \partial_p q' \rangle - \langle \omega' \cdot \partial_p q' \rangle + Res \tag{1}$$

where, P (mm/day), V (m/s), ω (Pa/s), and q (g/g) are the precipitation, horizontal winds, vertical velocity, and specific humidity, respectively. The overbar denotes the reference state of the piControl experiments, while a prime denotes the departure of these variables from the reference state. $\langle * \rangle$ represents a mass integration from surface to 100 hPa. The anomalous precipitation is balanced by anomalous evaporation (the first term on the right-hand of Eq. (1)), anomalous horizontal moisture transport (the third to four terms on the right-hand of Eq. (1)), and vertical moisture transport (the fifth to seventh terms on the right-hand of Eq. (1)). The last term *Res* is the residual term. As shown in Fig. 4a, the reduced DJF rainfall over the Amazon basin is primarily attributed to the vertical moisture gradient transported by anomalous vertical motion (i.e., dynamical processes), and is partially offset by the increased humidity (i.e., thermodynamical processes). Compared to these two terms, other processes (e.g., evaporation) are weak and the residual term is negligible.

The dominant processes that contribute to the asymmetric rainfall response are further examined in Fig. 4b and c, which show the differences in the mid-tropospheric vertical velocity and lower-tropospheric specific humidity. Due to the irreversible response of surface temperature (Qu and Huang, 2023; Zhang et al., 2023), a warmer atmosphere during the RD period can hold more water vapor (Fig. 4c). In the Amazon basin, where ascent prevails climatologically, more water vapor contributes to enhance precipitation, which reflects the "wet-get-wetter" mechanism (Chou et al., 2009; Held and Soden, 2006). However, the above thermodynamic process is not the whole story, and not all places with increased moisture have seen an increase in rainfall. Particularly, the decreased rainfall over the Amazon basin is mainly due to the dynamical process, with an anomalous strong descending motion (Fig. 4b). This descending motion overcomes the contribution of increased moisture and becomes the direct cause of the asymmetric response of the Amazon rainfall.

2.3. *Dynamical mechanisms responsible for the irreversible response*

2.3.1. *The role of zonal circulation and equatorial Pacific SST*

To scrutinize the mechanisms generating anomalous descending motion over the Amazon basin, Fig. 5a and b il-

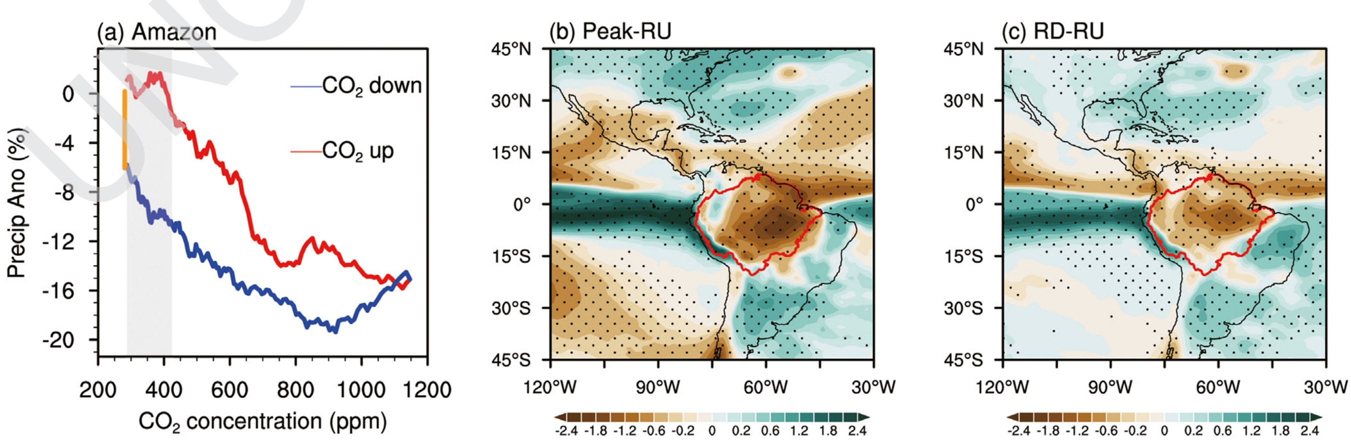

Fig. 3 – (a) Evolution of DJF mean rainfall anomalies (%) over the Amazon basin corresponding to CO_2 concentration during the CO_2 ramp-up (red), ramp-down (blue), and restoring (orange) periods. Spatial pattern of MME difference in DJF mean rainfall (unit: mm/day) between the (b) CO_2 peak (101–140) and RU (1–40) periods, (c) RD (241–280) and RU (1–40) periods. The dotted area passes the model sign consistency test (six out of nine) and 90 % significance test for difference in mean. (For interpretation of the references to color in this figure legend, the reader is referred to the web version of this article.) Q4

Please cite this article as: Suqin Zhang, Xia Qu, Gang Huang et al., Reduced rainfall over the Amazon basin in an idealized CO2 removal scenario: Remote dynamic processes, Journal of Environmental Sciences, https://doi.org/10.1016/j.jes.2024.05.035

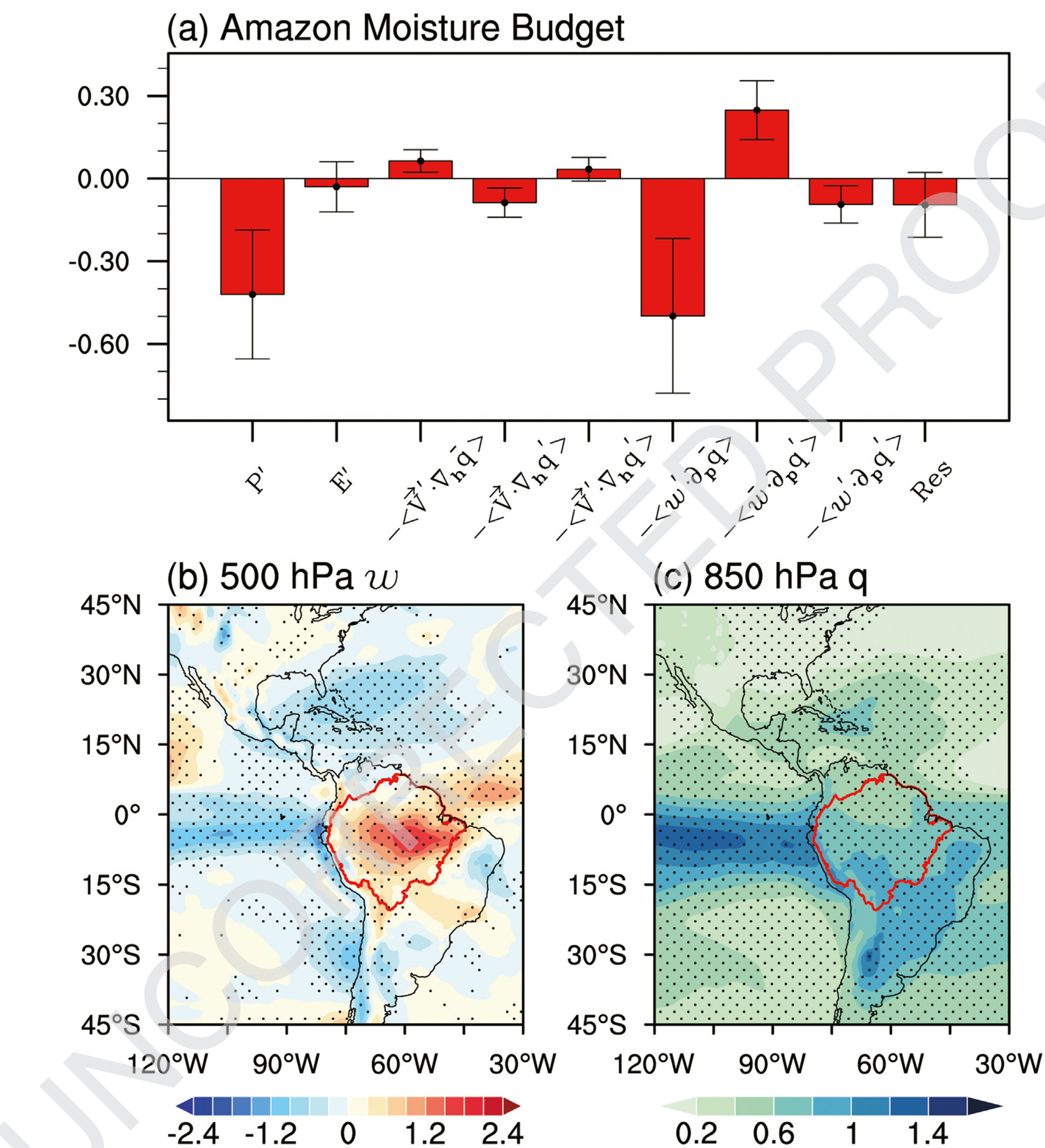

Fig. 4 – (a) The difference in the terms of the moisture budget equation (unit: mm/day) between RD (241–280) and RU (1–40) periods. Error bars indicate the inter-model uncertainty (1.96 x standard deviation). (b) The difference in the vertical velocity (unit: 10^{-2} Pa/s) at 500 hPa between the RD and RU periods. The dotted area passes the model sign consistency test (six out of nine). (c) The same as (b), but for the specific humidity (unit: g/kg) at the 850 hPa.

lustrate large-scale divergent circulation in the upper and lower troposphere. Following the Helmholtz theorem (Holton and Hakim, 2013), horizontal velocity can be decomposed into rotational and divergent parts, where only the latter associates with vertical motion. Fig. 5a and b reveal lower-tropospheric convergence and upper-tropospheric divergence over the equatorial eastern Pacific, accompanied by anomalous upper-tropospheric convergence and low-tropospheric divergence over the Amazon basin. This feature aligns with the zonal circulation cell depicted in Fig. 5c, featuring anomalous ascending motion over the eastern Pacific and descending motion over the Amazon basin. Therefore, subsidence over the Amazon is potentially linked to remote forcing over the equatorial Pacific Ocean.

The anomalous divergent circulation and zonal circulation cell shown in Fig. 5 resemble the observed mechanism by

Please cite this article as: Suqin Zhang, Xia Qu, Gang Huang et al., Reduced rainfall over the Amazon basin in an idealized CO2 removal scenario: Remote dynamic processes, Journal of Environmental Sciences, https://doi.org/10.1016/j.jes.2024.05.035

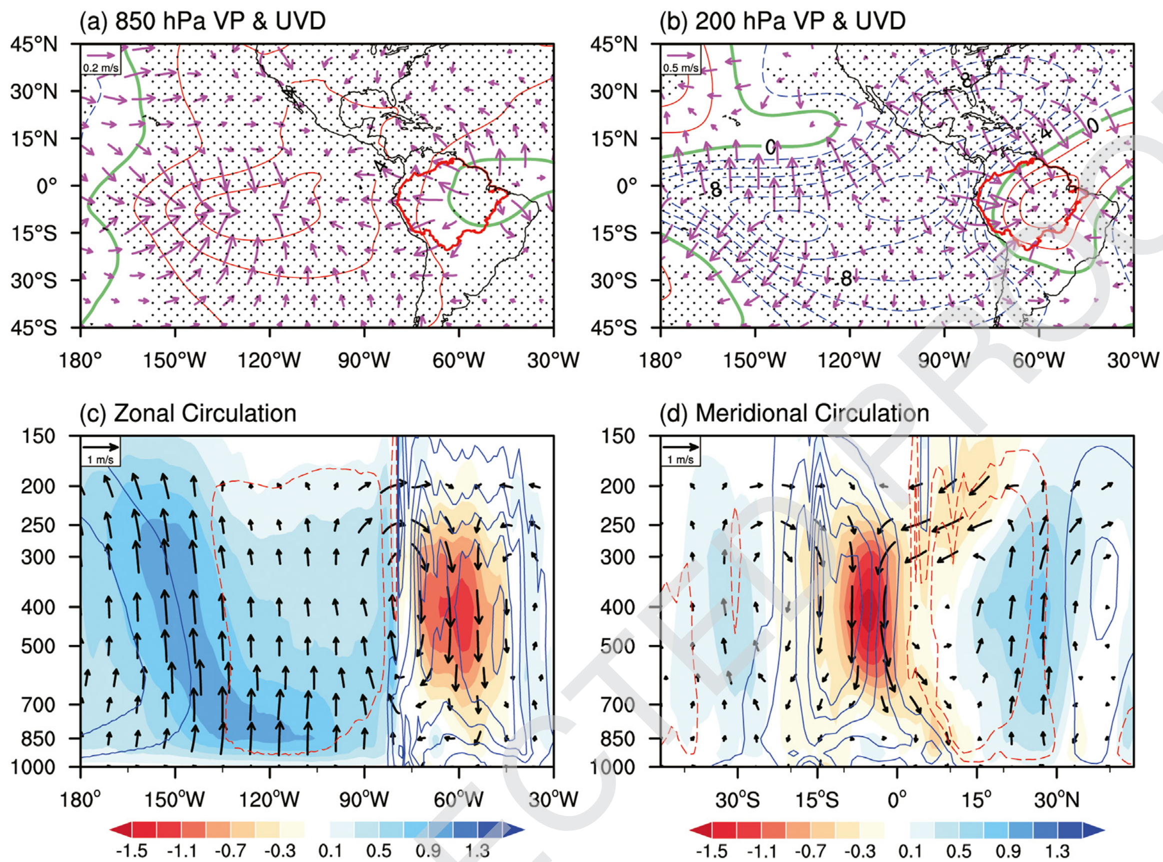

Fig. 5 – (a and b) Difference in velocity potential (color line; unit: 10^6 m^2/s) and divergence winds (vector; unit: m/s) at 850 hPa (a) and 200 hPa (b) between the RD (241–280) and RU (1–40) periods. Black dots and vectors shown denote the region that satisfies the model sign consistency. (c) Cross-section of differences in zonal and vertical velocities (vectors), averaged for 15.5°S–0.5°N between the RD and RU periods. (d) Same as (c), but for meridional and vertical velocities, averaged over 75°–50°W. Shaded values are differences in vertical velocities (unit: -10^{-2} Pa/s). Color contour line indicates climatological vertical velocities obtained from the last 100 years of the piControl experiment. (For interpretation of the references to color in this figure legend, the reader is referred to the web version of this article.)

which ENSO affects Amazon rainfall (Cai et al., 2020; Kay et al., 2022). Thus, Fig. 6 examines the SST anomalies in the Pacific Ocean for the RU and RD periods as well as their differences. During the RU period, there are anomalous warm SST anomalies over the equatorial central Pacific, consistent with El Niño-like SST pattern predicted under the global warming scenario (Cai et al., 2018, 2020). In the RD period, a more pronounced warming in the equatorial Pacific Ocean occurs due to the weakened Walker circulation and the attenuated upwelling (Chadwick et al., 2013; Song et al., 2022; Zhang et al., 2023). Therefore, compared to the RU period, an El Niño-like anomalous SST pattern is seen over the tropical Pacific Ocean during the RD period (Fig. 6c and Appendix A Fig. S3), consistent with recent studies under the CDR scenario (Liu et al., 2023; Pathirana et al., 2023; Zhou et al., 2022). This anomalous warm SST in the equatorial Pacific Ocean generate low-tropospheric convergence, ascending motion, and upper-tropospheric divergence (Fig. 5), which further affects the Amazon rainfall via the anomalous zonal circulation. Thus, the zonal circulation is recognized as the first pathway linking the Pacific Ocean warm SST anomalies to the reduced rainfall over the Amazon basin.

2.3.2. *The role of meridional circulation and Rossby wave train*

Apart from the anomalous zonal circulation, the anomalous meridional circulation also contributes to the anomalous descending motion over the Amazon basin. Fig. 5 reveals low-tropospheric convergence and upper-tropospheric divergence over the Sargasso Sea, accompanied by increased local rainfall (Fig. 3b). This induces anomalous ascending motion and upper-tropospheric northerly winds, leading to anomalous descending motion over the Amazon basin, forming an obvious meridional circulation cell (Fig. 5d). In-depth exploration of this meridional circulation is presented in Fig. 7, which shows the anomalous low-tropospheric circulation and the vertically integrated moisture transport. There appear anomalous southwesterly winds over the Amazon basin and the Caribbean Sea, which implies a slowdown of the climatological northeasterly trade winds and the cross-equatorial flow, as well as the moisture transport (Fig. 1c and d). This is consistent with the divergence of vertically integrated moisture fluxes (Fig. 7b) and the reduced rainfall (Fig. 3) over the Amazon basin. Notice that the anomalous southwesterly winds over the Caribbean Sea are part of

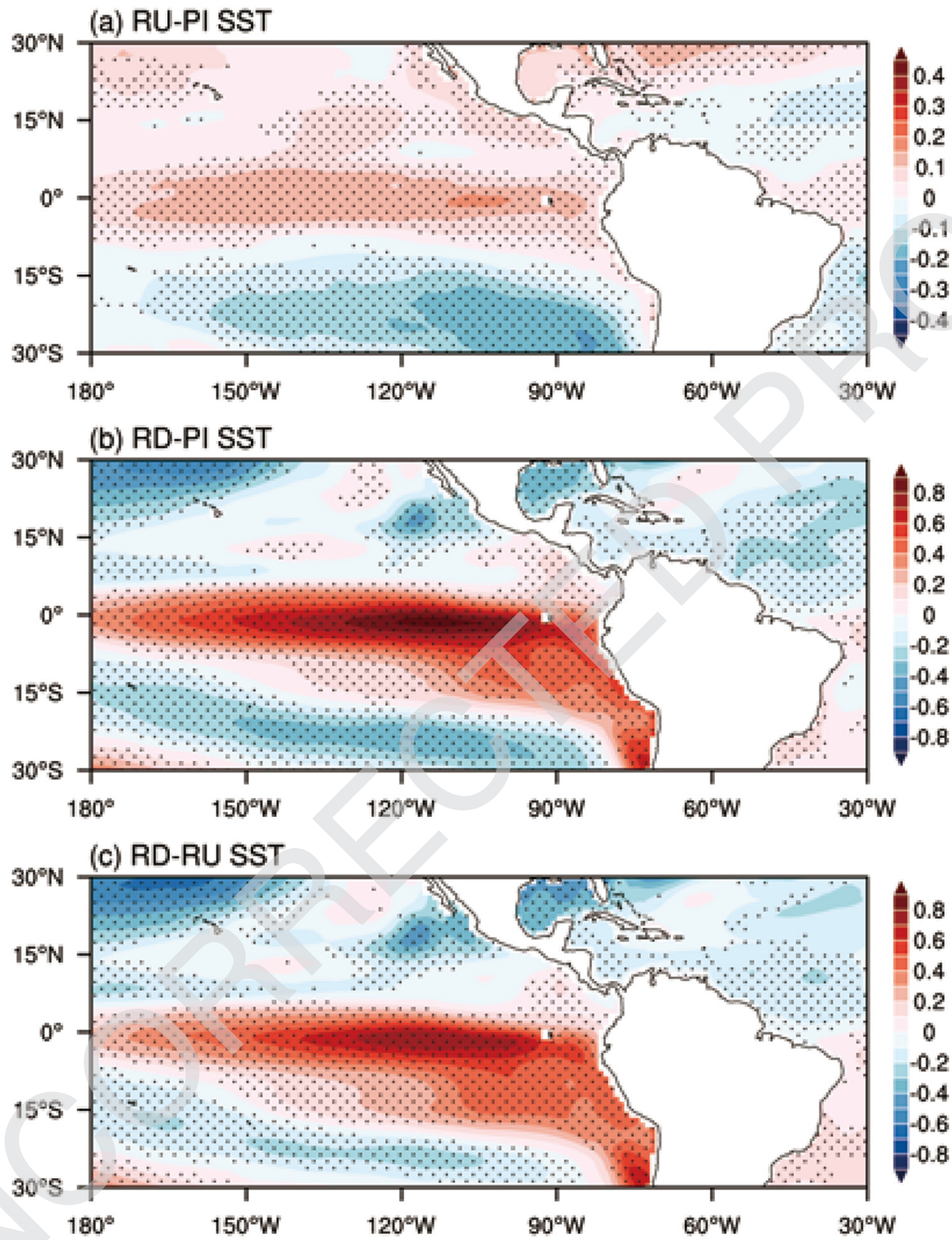

Fig. 6 – (a and b) SST anomalies (unit: K) with the tropical mean SST removed during the RU (a) and RD (b) periods compared to piControl, respectively. (c) Same as (a), but for the difference between the RD and RU periods. The dotted areas satisfy the model sign consistency.

an anomalous cyclone centered over the Florida Peninsula (Fig. 7a).

It is evident that the anomalous low-tropospheric cyclone over the Florida Peninsula and the increased rainfall over the Sargasso Sea are associated with the ascending branching of the local meridional circulation. Thus, the next question is, how they are generated? Fig. 8 shows the difference in the upper-troposphere stream function between the RD and RU periods. Two anomalous anticyclones appear over the tropical eastern Pacific Ocean, understood as the equatorial Rossby wave response to warm SST anomalies underneath (Gill, 1980; Matsuno, 1966). More importantly, there are alternative cyclones and anticyclones in the northern hemisphere, forming a stationary Rossby wave train. This argument is verified by the wave activity flux (Takaya and Nakamura, 2001), which can reflect the propagation of Rossby wave energy. However, the wave activity flux is derived under the assumption of quasi-geostrophic balance, which may not be fully applicable in the Tropics. Therefore, the Rossby ray tracings (Karoly, 1983; Shaman and Tziperman, 2005) are employed to further detect the stationary Rossby wave train. As shown in Fig. 8, both the wave activity flux and the Rossby ray tracings reflect a northeastward wave energy propagation from the tropical northeastern Pacific to the southern United States of America (USA), and then turn southeast to reach the tropical North Atlantic.

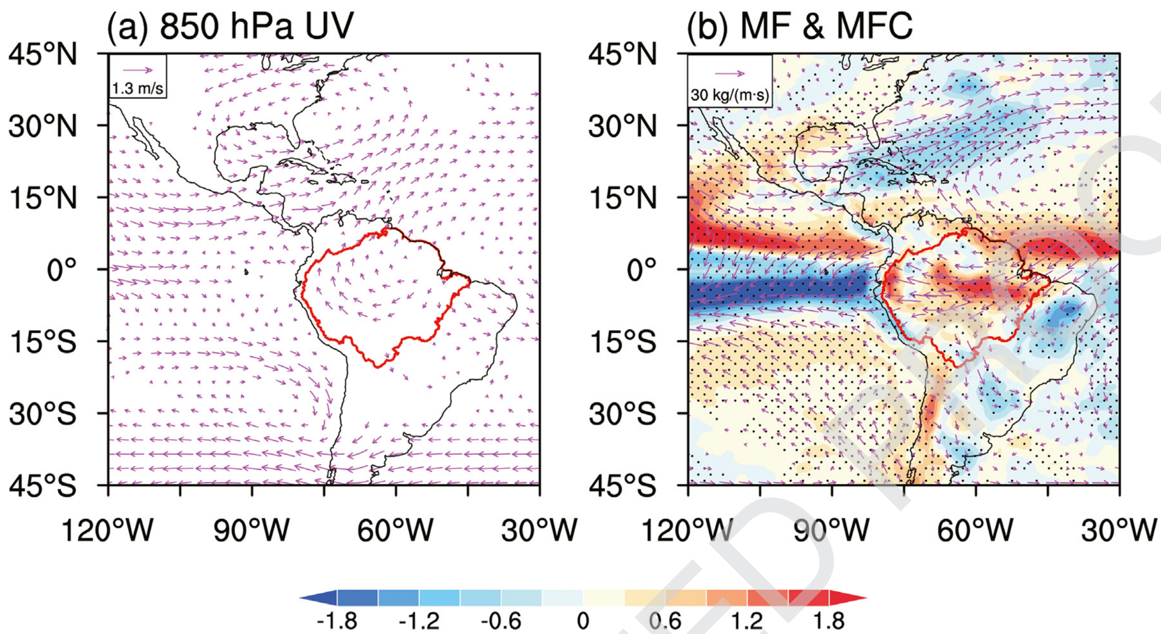

Fig. 7 – (a) Spatial difference in the 850 hPa winds (unit: m/s) between the RD (241–280) and RU (1–40) periods. (b) Same as (a), but for the vertically integrated moisture fluxes from the surface to 100 hPa (vector; unit: 10^2 kg/(m•s)) and their divergence (shading; unit: 10^{-5} kg/(m^2•s). The vectors shown and the dotted area satisfy the model sign consistency test.

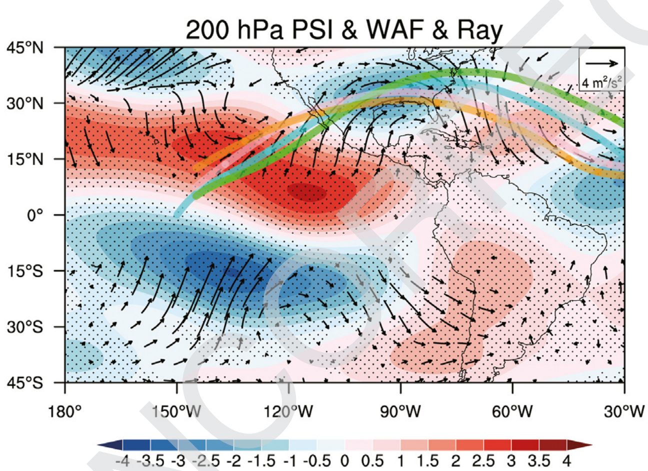

Fig. 8 – Response of the stream function (shading; unit: 10^6 m^2/s), wave activity flux (vector; unit: m^2/s^2), and wave ray trajectory (colored lines) at 200 hPa during RD compared to the RU period. DJF climatology during the RU period is the baseline. Stream function with zonal mean removed. Wave activity flux values within 10° of the equators are omitted. Path of a Rossby ray, starting with an initial zonal wavenumber 5 (pink, orange) and 6 (blue, green) at 7.5°N, 145°W (pink), and 12.5°N, 145°W (orange), and 0°, 150°W (blue), and 2.5°N, 145°W (green). The vectors shown and the dotted area satisfy the model sign consistency. (For interpretation of the references to color in this figure legend, the reader is referred to the web version of this article.)

Noteworthy is the anomalous upper-tropospheric cyclone over the southern USA (Fig. 8), slightly westward relative to the low-tropospheric cyclone (Fig. 7a). Such a slightly westward phase tilt is a common feature of the Rossby wave train, which may be linked to the energy conversion from the basic flow (Chen et al., 2020; Hu et al., 2023). The increased rainfall and ascending motion over the Sargasso Sea are located east of the upper-tropospheric cyclone, explained by the quasi-geostrophic omega equation (Gu et al., 2018; Holton and Hakim, 2013). Because the basic flow is westerly, positive vorticity advection and warm advection tend to occur east of the upper-tropospheric cyclone anomaly, favoring ascending motion over the Sargasso Sea. Once ascending motion appears, it can be further enhanced by the diabatic heating related to the increased rainfall, leading to positive feedback (e.g., Gu et al., 2018). Consequently, ascending motion over the Sargasso Sea and sinking over the Amazon basin form a local meridional circulation (Fig. 5). As the climatological rainfall over the Amazon basin is large, giving rise to robust rainfall-circulation feedback. Anomalous descendance can reduce the rainfall, leading to a cooling anomaly that, in turn, amplifies the anomalous descendance. Similar mechanisms were elucidated in Wu et al. (2010). This feedback loop results in an easier occurrence of a sink anomaly over the Amazon basin. Therefore, beyond the anomalous zonal circulation, another pathway linking warm Pacific SST anomalies and decreased Amazon rainfall is the Rossby wave train and meridional circulation.

3. Summary and discussion

The Amazon basin, encompassing approximately 40 % of global tropical forests, stands as the world's largest river basin. Essential to these tropical ecosystems is the region's copious rainfall, typically exceeding 2000 mm/year. Numerous studies have delved into the factors influencing Amazon rainfall un-

Please cite this article as: Suqin Zhang, Xia Qu, Gang Huang et al., Reduced rainfall over the Amazon basin in an idealized CO2 removal scenario: Remote dynamic processes, Journal of Environmental Sciences, https://doi.org/10.1016/j.jes.2024.05.035

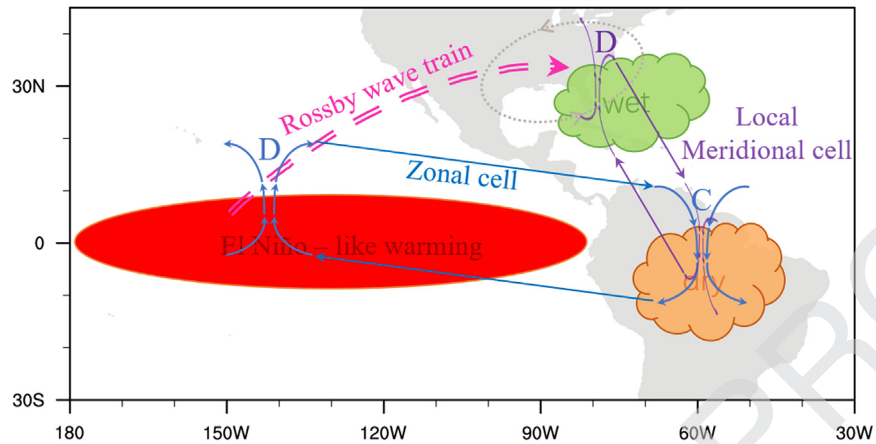

Fig. 9 – Schematic diagram shows key processes considered in this study, by which the DJF mean rainfall over the Amazon exhibits an irreversible response, with anomalous drought. Red shading, orange shading, and green shading indicate the enhanced El Niño-like SST anomalies, the anomalous drought over the Amazon, and the anomalous wetting over the Caribbean during the RD period compared to the RU period, respectively. Blue arrows represent the zonal circulation. Double-dashed arrows denote the stationary Rossby wave train. Purple arrows indicate the local meridional circulation.

der current climatic conditions and its alterations in the face of global warming. This manuscript investigates the evolution of Amazon rainfall under an idealized CDR scenario, with particular attention to its asymmetric response. CMIP6 simulations highlight that, when the atmospheric CO_2 is removed to pre-industrial level, the Amazon basin could experience anomalous drought during the following 60 years.

The mechanisms behind this reduced Amazon rainfall are synthesized in Fig. 9. The moisture budget analysis underscores that the reduced rainfall mainly resulted from a dynamical process involving anomalous descending, which overrides the thermodynamical effect of increased moisture. The fundamental cause of this anomalous descending motion lies in an El Niño-like SST pattern in the Pacific Ocean. On the one hand, this anomalous SST pattern directly affect the Amazon rainfall through the anomalous zonal circulation—air ascends over the equatorial eastern Pacific and descends over the Amazon basin. On the other hand, it indirectly modulates Amazon rainfall via the Rossby wave train and meridional circulation. Corresponding to the warm equatorial eastern Pacific, a northeast-southeast propagating Rossby wave train is excited, leading to an upper-level anomalous cyclone over the southern USA. Consequently, an anomalous meridional circulation emerges, with an ascending branch in the Sargasso Sea and a descending branch over the Amazon basin.

If the idealized CDR pathway is implemented, the Amazon basin may experience anomalous drought. Reduced rainfall can greatly affect nutrient input into Amazon basin rivers and other freshwater systems, impacting both the environment and the people who rely on these resources (Parmesan et al., 2022; CLS, 2024). For instance, droughts can isolate fish populations, making migration and genetic diversity maintenance challenging. Additionally, reduced rainfall can exacerbate positive feedback among drought, deforestation, and wildfires, leading to reduced biodiversity and weaker carbon sequestration, which, in turn, contributes to global warming (Wang and Huang, 2022; Zemp et al., 2017). Staal et al. (2020a) indicates that the deforestation tends to increase 0.13 % per year with every mm of water deficit. Deforestation, in turn, has caused an estimated 4 % of the recent observed drying. Therefore, when assessing the climate effects of CDR, it's crucial to consider the impact of secondary hazards.

Since most of the models participating in the CDR experiment only conducted 60 years of restoring period, we cannot analyze how long it will take for precipitation in Amazon basin to fully recover. Such temporary reduction in Amazon basin rainfall have been attributed to an enhanced El Niño-like SST pattern in the Pacific Ocean, which is the result of the asymmetric response of the ocean heat uptake. The oceans absorb heat until the middle of the CO_2 ramp-down period; after that, the oceans continue to release heat (Yeh et al., 2021). Correspondingly, slow SST-driven response lags the evolution of CO_2 concentration remarkably, and dominates the total climate response during the CO_2 ramp-down period (Zhang et al., 2024; Zhou et al., 2022). The contribution of slow response ocean, as well as ocean heat uptake continue to diminish during the CO_2 restoring period. If a restoring period is maintained long enough, the reduced rainfall in the Amazon basin will gradually recover as the contribution of the slow response diminishes.

Situated in the South American monsoon region, the Amazon basin's rainfall is intricately linked to the onset and retreat of the monsoon. Whether the weakened rainfall over the Amazon basin means a shorter rainy season is an important question that needs to be investigated. Moon and Ha (2020) projected a shorter rainy season over the South American monsoon region under the global warming scenario due to advanced retreat and delayed onset. Investigating the response of the Amazon's rainy season length under the CDR scenario is a focal point for future research.

Uncited references

Q5

Liu et al., 2022, Baidya and Avissar, 2002, Staal et al., 2020b, Brando et al., 2014.

Declaration of competing interest

The authors declare that they have no known competing financial interests or personal relationships that could have appeared to influence the work reported in this paper.

CRediT authorship contribution statement

Suqin Zhang: Writing – review & editing, Writing – original draft, Formal analysis, Data curation, Conceptualization. **Xia Qu:** Writing – review & editing, Supervision, Project administration, Funding acquisition, Formal analysis. **Gang Huang:** Writing – review & editing, Supervision, Project administration, Funding acquisition. **Peng Hu:** Writing – review & editing, Writing – original draft, Supervision, Formal analysis, Conceptualization.

Acknowledgments

This work was supported by the National Natural Science Foundation of China (nos. 42141019, 42175055, 42261144687), the second Tibetan Plateau Scientific Expedition and Research program (no. 2019QZKK0102), and the project of the key Laboratory of Meteorological Disaster, Ministry of Education & Collaborative Innovation Center on Forecast and Evaluation of Meteorological Disaters, Nanjing University of Information Science & Technology (no. KLME202111). The authors thank the World Climate Research Program, the climate modeling groups, and the Earth System Grid Federation.

Supplementary materials

Supplementary material associated with this article can be found, in the online version, at doi:10.1016/j.jes.2024.05.035.

References

Adam, O., Schneider, T., Brient, F., 2018. Regional and seasonal variations of the double-ITCZ bias in CMIP5 models. Clim. Dyn. 51, 101–117.
Adams, H.D., Zeppel, M.J.B., Anderegg, W.R.L., Hartmann, H., Landhäusser, S.M., Tissue, D.T., et al., 2017. A multi-species synthesis of physiological mechanisms in drought-induced tree mortality. Nat. Ecol. Evol. 1, 1285–1291.
Adler, R.F., Sapiano, M.R.P., Huffman, G.J., Wang, J.J., Gu, G.J., Bolvin, D., et al., 2018. The Global Precipitation Climatology Project (GPCP) monthly analysis (new version 2.3) and a review of 2017 global precipitation. Atmosphere (Basel) 9, 138.
Almazroui, M., Ashfaq, M., Islam, M.N., Rashid, I.U., Kamil, S., Abid, M.A., et al., 2021. Assessment of CMIP6 performance and projected temperature and precipitation changes over South America. Earth Syst. Environ. 5, 155–183.
Baidya, R.S., Avissar, R., 2002. Impact of land use/land cover change on regional hydrometeorology in Amazonia. J. Geophys. Res. Atmos. 107, LBA–LB4.
Bréda, N., Huc, R., Granier, A., Dreyer, E., 2006. Temperate forest trees and stands under severe drought: a review of eco-physiological responses, adaptation processes and long-term consequences. Ann. For. Sci. 63, 625–644.
Boulton, C.A., Lenton, T.M., Boers, N., 2022. Pronounced loss of Amazon rainforest resilience since the early 2000s. Nat. Clim. Change 12, 271–278.
Brando, P.M., Balch, J.K., Nepstad, D.C., Morton, D.C., Puta, F.E., Coe, M.T., et al., 2014. Abrupt increases in Amazonian tree mortality due to drought-fire interactions. Proc. Natl. Acad. Sci. USA. 111, 6347–6352.
Burleyson, C.D., Feng, Z., Hagos, S.M., Fast, J., Machado, L.A.T., Martin, S.T., 2016. Spatial variability of the background diurnal cycle of deep convection around the GoAmazon2014/5 field campaign sites. J. Appl. Meteorol. Climatol. 55, 1579–1598.
Cai, W.J., Wang, G.J., Dewittw, B., Wu, L.L., Santoso, A., Takahashi, K., 2018. Increased variability of eastern Pacific El Niño under greenhouse warming. Nature 564, 201–206.
Cai, W.J., McPhaden, M.J., Crimm, A.M., Rodrigues, R.R., Taschetto, A.S., Garreaud, R.D., et al., 2020. Climate impacts of the El Niño–Southern Oscillation on South America. Nat. Rev. Earth Environ. 1, 215–231.
Cao, L., Jin, X.Y., Jiang, J., 2023. Simulated carbon cycle and Earth system response to atmospheric CO_2 removal. Adv. Clim. Change Res. 14, 313–321.
Chadwick, R., Wu, P.L., Good, P., Andrews, T., 2013. Asymmetries in tropical rainfall and circulation patterns in idealised CO_2 removal experiments. Clim. Dyn. 40, 295–316.
Chen, S.F., Wu, R.G., Chen, W., Hu, K.M., Yu, B., 2020. Structure and dynamics of a springtime atmospheric wave train over the North Atlantic and Eurasia. Clim. Dyn. 54, 5111–5126.
Chou, C., Neelin, J.D., Chen, C.A., Tu, J.Y., 2009. Evaluating the "Rich-Get-Richer" mechanism in tropical precipitation change under global warming. J. Clim. 22, 1982–2005.
Ciemer, C., Rehm, L., Kurths, J., Donner, R.V., Winkelmann, R., Boers, N., 2020. An early-warning indicator for Amazon droughts exclusively based on tropical Atlantic sea surface temperatures. Environ. Res. Let. 15, 094087.
CLS (Climate Last Stand), 2024. Amazon Rainforest Climate Change: facts & Impact Available:. https://www.climatelaststand.com/amazon-rainforest-climate-change/ Accessed April 24, 2024.
Danabasoglu, G., Lamarque, J.F., Bacmeister, J., Bailey, D.A., DuVivier, A.K., Edwards, J., et al., 2020. The community earth system model version 2 (CESM2). J. Adv. Model. Earth. Syst. 12, e2019MS001916.
Doughty, C.E., Metcalfe, D.B., Girardin, C.A., Amezquita, F.F., Cabrera, D.G., Huasco, W.H., et al., 2015. Drought impact on forest carbon dynamics and fluxes in Amazonia. Nature 519, 78–82.
Dunne, J.P., Horowitz, L.W., Adcroft, A.J., Ginoux, P., Held, I.M., John, J.G., et al., 2020. The GFDL earth system model version 4.1 (GFDL-ESM 4.1): overall coupled model description and simulation characteristics. J. Adv. Model. Earth Syst. 12, e2019MS002015.
Durán-Quesada, A.M., Reboita, M., Gimeno, L., 2012. Precipitation in tropical America and the associated sources of moisture: a short review. Hydrol. Sci. J. 57, 612–624.
Eyring, V., Bony, S., Meehl, G.A., Senior, C.A., Stevens, B., Stouffer, R.J., et al., 2016. Overview of the coupled model intercomparison project phase 6 (CMIP6) experimental design and organization. Geosci. Model Dev. 9, 1937–1958.
Fassoni-Andrade, A.C., Fleischmann, A.S., Papa, F., Paiva, R.C.D.d., Wongchuig, S., Melack, J.M., et al., 2021. Amazon hydrology from space: scientific advances and future challenges. Rev. Geophys. 59, e2020RG000728.
Feldpausch, T.R., Phillips, O.L., Brienen, R.J.W., Gloor, E., Lioyd, J., Lopez-Gonzalez, G., et al., 2016. Amazon forest response to repeated droughts. Glob. Biogeochem. Cycles 30, 964–982.
Fu, R., Yin, L., Li, W.H., Arias, P.A., Dickinson, R.E., Huang, L., et al., 2013. Increased dry-season length over southern Amazonia in recent decades and its implication for future climate projection. Proc. Natl. Acad. Sci. USA. 110, 18110–18115.

Gill, A.E., 1980. Some simple solutions for heat-induced tropical circulation. Q. J. R. Meteorol. Soc. 106, 447–462.
Gu, W., Wang, L., Hu, Z.Z., Hu, K.M., Li, Y., 2018. Interannual variations of the first rainy season precipitation over South China. J. Clim. 31, 623–640.
Hajima, T., Watanabe, M., Yamamoto, A., Tatebe, H., Noguchi, M.A., Abe, M., et al., 2020. Development of the MIROC-ES2L Earth system model and the evaluation of biogeochemical processes and feedbacks. Geosci. Model Dev. 13, 2197–2244.
Held, I.M., Soden, B.J., 2006. Robust responses of the hydrological cycle to global warming. J. Clim. 19, 5686–5699.
Holton, J.R., Hakim, G.J., 2013. An Introduction to Dynamic Meteorology, 5th Edition ed.
Hu, P., Chen, W., Chen, S.F., Wang, L., Liu, Y.Y., 2023. Impacts of Pacific Ocean SST on the interdecadal variations of tropical Asian summer monsoon onset: new eastward-propagating mechanisms. Clim. Dyn. 61, 4733–4748.
IPCC, 2021. Climate Change 2021 – The Physical Science Basis: Working Group I Contribution to the Sixth Assessment Report of the Intergovernmental Panel on Climate Change. Cambridge University Press.
Kanamitsu, M., Ebisuzaki, W., Woollen, J., Yang, S.K., Hnilo, J.J., Fiorino, M., et al., 2002. NCEP-DOE AMIP-II reanalysis (R-2). Bull. Am. Meteorol. Soc. 83, 1631–1643.
Karoly, D.J., 1983. Rossby wave propagation in a barotropic atmosphere. Dyn. Atmosph. Ocean. 7, 111–125.
Kay, G., Dunstone, N.J., Smith, D.M., Betts, R.A., Cunningham, C., Scaife, A.A., 2022. Assessing the chance of unprecedented dry conditions over North Brazil during El Niño events. Environ. Res. Lett. 17, 064016.
Keller, D.P., Lenton, A., Scott, V., Vaughan, N.E., Bauer, N., Ji, D.Y., et al., 2018. The carbon dioxide removal model intercomparison project (CDRMIP): rationale and experimental protocol for CMIP6. Geosci. Model Dev. 11, 1133–1160.
Khanna, J., Medvigy, D., Fisch, G., de Araújo Tiburtino Neves, T.T., 2018. Regional hydroclimatic variability due to contemporary deforestation in southern Amazonia and associated boundary layer characteristics. J. Geophys. Res. Atmos. 123, 3993–4014.
Kim, S.K., Shin, J., An, S.I., Kim, H.J., Im, N., Xie, S.P., et al., 2022. Widespread irreversible changes in surface temperature and precipitation in response to CO_2 forcing. Nat. Clim. Change 12, 834–840.
Kug, J.S., Oh, J.H., An, S.I., Yeh, S.W., Min, S.K., Son, S.W., et al., 2022. Hysteresis of the intertropical convergence zone to CO_2 forcing. Nat. Clim. Change 12, 47–53.
Leite-Filho, A.T., Soares-Filho, B.S., Davis, J.L., Abrahão, G.M., Börner, J., 2021. Deforestation reduces rainfall and agricultural revenues in the Brazilian Amazon. Nat. Commun. 12, 2591.
Li, Y., Brando, P.M., Morton, D.C., Lawrence, D.M., Yang, H., Randerson, J.T., 2022. Deforestation-induced climate change reduces carbon storage in remaining tropical forests. Nat. Commun. 13, 1964.
Liebmann, B., Kiladis, G.N., Carvalho, L.M.V., Jones, C., Vera, C.S., Bladé, I., et al., 2009. Origin of convectively coupled Kelvin waves over South America. J. Clim. 22, 300–315.
Liu, C., An, S.I., Jin, F.F., Shin, J., Kug, J.S., Zhang, W.J., et al., 2023. Hysteresis of the El Niño–southern oscillation to CO_2 forcing. Sci. Adv. 9, eadh8442.
Liu, F., Wang, B., Ouyang, Y., Wang, H., Qiao, S.B., Chen, G.S., et al., 2022. Intraseasonal variability of global land monsoon precipitation and its recent trend. npj Clim. Atmos. Sci. 5, 30.
Llopart, M., Simões Reboita, M., da Rocha, R.P., 2020. Assessment of multi-model climate projections of water resources over South America CORDEX domain. Clim. Dyn. 54, 99–116.
Marengo, J.A., Liebmann, B., Grimm, A.M., Mista, V., Silva Dias, P.L., Cavalvanti, I.F.A., et al., 2012. Recent developments on the South American monsoon system. Int. J. Climatol. 32, 1–21.
Matsuno, T., 1966. Quasi-geostrophic motions in the equatorial area. J. Meteorol. Soc. Japan 44, 25–43.
Mayta, V.C., Adames, Á.F., 2023. Moist thermodynamics of convectively coupled waves over the western hemisphere. J. Clim. 36, 2765–2780.
Mayta, V.C., Adames, Á.F., Ahmed, F., 2022. Westward-propagating moisture mode over the tropical Western Hemisphere. Geophys. Res. Lett. 49, e2022GL097799.
Mayta, V.C., Silva, N.P., Ambrizzi, T., Dias, P.L.S., Espinoza, J.C., 2020. Assessing the skill of all-season diverse Madden–Julian oscillation indices for the intraseasonal Amazon precipitation. Clim. Dyn. 54, 3729–3749.
Mayta, V.C., Kiladis, G.N., Dias, J., Silva Dias, P.L., Gehne, M., 2021. Convectively coupled Kelvin waves over tropical South America. J. Clim. 34, 6531–6547.
McDowell, N., Pockman, W.T., Allen, C.D., Breshears, D.D., Cobb, N., Kolb, T., et al., 2008. Mechanisms of plant survival and mortality during drought: why do some plants survive while others succumb to drought? New Phytol 178, 719–739.
McGregor, S., Cassou, C., Kosaka, Y., Phillips, A.S., 2022. Projected ENSO teleconnection changes in CMIP6. Geophys. Res. Lett. 49, e2021GL097511.
McGuffie, K., Henderson-Sellers, A., Zhang, H., Durbidge, T.B., Pitman, A.J., 1995. Global climate sensitivity to tropical deforestation. Glob. Planet. Change. 10, 97–128.
Moon, S., Ha, K.J., 2020. Future changes in monsoon duration and precipitation using CMIP6. npj Clim. Atmos. Sci. 3, 45.
Muñoz, Á.G., Goddard, L., Robertson, A.W., Kushnir, Y., Baethgen, W., 2015. Cross–time scale interactions and rainfall extreme events in Southeastern South America for the Austral Summer. Part I: potential predictors. J. Clim. 28, 7894–7913.
Parmesan, C., Morecroft, M.D., Trisurat, Y., Adrian, R., Anshari, G.Z., Arneth, A., et al., 2022. Terrestrial and freshwater ecosystems and their services. In: Pörtner, H.-O., Roberts, D.C., Tignor, M., Poloczanska, E.S., Mintenbeck, K., Alegría, A., et al. (Eds.), Climate Change 2022: Impacts, Adaptation and Vulnerability. Contribution of Working Group II to the Sixth Assessment Report of the Intergovernmental Panel on Climate Change, Cambridge, UK and New York, NY, USA. Cambridge University Press, pp. 197–377.
Park, S.W., Kug, J.S., 2022. A decline in atmospheric CO_2 levels under negative emissions may enhance carbon retention in the terrestrial biosphere. Commun. Earth Environ. 3, 289.
Pascale, S., Carvalho, L.M.V., Adams, D.K., Castro, C.L., Cavalcanti, I.F.A., 2019. Current and future variations of the Monsoons of the Americas in a warming climate. Curr. Clim. Change Rep. 5, 125–144.
Pathirana, G., Oh, J.H., Cai, W.J., An, S.I., Min, S.K., Jo, S.Y., 2023. Increase in convective extreme El Niño events in a CO_2 removal scenario. Sci. Adv. 9, eadh2412.
Qu, X., Huang, G., 2023. The primary factors influencing the cooling effect of carbon dioxide removal. npj Clim. Atmos. Sci. 6, 215.
Qu, X., Huang, G., Hu, K.M., Xie, S.P., Du, Y., Zheng, X.T., et al., 2015. Equatorward shift of the South Asian high in response to anthropogenic forcing. Theo. Appl. Climatol. 119, 113–122.
Rayner, N.A., Parker, D.E., Horton, E.B., Folland, C.K., Alexander, L.V., Rowell, D.P., et al., 2003. Global analyses of sea surface temperature, sea ice, and night marine air temperature since the late nineteenth century. J. Geophys. Res. Atmos. 108, 4407.
Reboita, M.S., Ambrizzi, T., Crespo, N.M., Dutra, L.M.M., Ferreira, G.W.D., Rehbein, A., et al., 2021. Impacts of teleconnection patterns on South America climate. Ann. N. Y. Acad. Sci. 1504, 116–153.
Salati, E., Dall'Olio, A., Matsui, E., Gat, J.R., 1979. Recycling of water in the Amazon Basin: an isotopic study. Water Resour. Res. 15 (5), 1250–1258.

Séférian, R., Nabat, P., Michou, M., Saint-Martin, D.S., Voldoire, A., Colin, J., et al., 2019. Evaluation of CNRM earth system model, CNRM-ESM2-1: role of earth system processes in present-day and future climate. J. Adv. Model. Earth. Syst. 11, 4182–4227.

Seland, Ø., Bentsen, M., Olivié, D., Toniazzo, T., Gjermundsen, A., Graff, L.S., et al., 2020. Overview of the Norwegian Earth System Model (NorESM2) and key climate response of CMIP6 DECK, historical, and scenario simulations. Geosci. Model Dev. 13, 6165–6200.

Senior, C.A., Jones, C.G., Wood, R.A., Sellarm, A., Belcher, S., Klein-Tank, A., et al., 2020. U.K. community earth system modeling for CMIP6. J. Adv. Model. Earth. Syst. 12, e2019MS002004.

Shaman, J., Tziperman, E., 2005. The Effect of ENSO on Tibetan Plateau snow depth: a stationary wave teleconnection mechanism and implications for the South Asian Monsoons. J. Clim. 18, 2067–2079.

Si, W., Liu, H.L., Zhang, X.X., Zhang, M.H., 2021. Double Intertropical Convergence Zones in Coupled Ocean-Atmosphere Models: progress in CMIP6. Geophys. Res. Lett. 48, e2021GL094779.

Song, S.Y., Yeh, S.W., An, S.I., Kug, J.S., Min, S.K., Son, S.W., Shin, J., 2022. Asymmetrical response of summer rainfall in East Asia to CO_2 forcing. Sci. Bull. 67, 213–222.

Staal, A., Fetzer, I., Wang-Erlandsson, L., Bosmans, J.H.C., Dekker, S.C., van Nes, E.H., et al., 2020. Hysteresis of tropical forests in the 21st century. Nat. Commun. 11, 4978.

Staal, A., Flores, B.M., Aguiar, A.P.D., Bosmans, J.H.C., Fetzer, I., Tuinenburg, O.A., 2020. Feedback between drought and deforestation in the Amazon. Environ. Res Lett. 15, 044024.

Swart, N.C., Cole, J.N.S., Kharin, V.V., Lazare, M., Scinocca, J.F., Gillett, N.P., et al., 2019. The Canadian earth system model version 5 (CanESM5.0.3). Geosci. Model Dev. 12, 4823–4873.

Takaya, K., Nakamura, H., 2001. A formulation of a phase-independent wave-activity flux for stationary and migratory quasigeostrophic Eddies on a zonally varying basic flow. J. Atmos. Sci. 58, 608–627.

Tang, S.Q., Xie, S.C., Zhang, Y.Y., Zhang, M.H., Schumacher, C., Upton, H., et al., 2016. Large-scale vertical velocity, diabatic heating and drying profiles associated with seasonal and diurnal variations of convective systems observed in the GoAmazon2014/5 experiment. Atmos. Chem. Phys. 16, 14249–14264.

Thakur, M.P., Reich, P.B., Hobbie, S.E., Stefanski, A., Rich, R., Rice, K.E., et al., 2018. Reduced feeding activity of soil detritivores under warmer and drier conditions. Nat. Clim. Change 8, 75–78.

Thome Sena, A.C., Magnusdottir, G., 2020. Projected end-of-century changes in the South American Monsoon in the CESM large ensemble. J. Clim. 33, 7859–7874.

Torres, R.R., Benassi, R.B., Martins, F.B., Lapola, D.M., 2021. Projected impacts of 1.5 and 2°C global warming on temperature and precipitation patterns in South America. Int. J. Clim. 42, 1597–1611.

Towner, J., Cloke, H.L., Lavado, W., Santini, W., Bazo, J., Coughlan de Perez, E., et al., 2020. Attribution of Amazon floods to modes of climate variability: a review. Meteoro. Appl. 27, e1949.

Wang, Y.F., Huang, P., 2022. Potential fire risks in South America under anthropogenic forcing hidden by the Atlantic Multidecadal Oscillation. Nat. Commun. 13, 2437.

Wu, P.L., Wood, R., Ridley, J., Lowe, J., 2010. Temporary acceleration of the hydrological cycl e in response to a CO_2 rampdown. Geophy. Res. Lett. 37, L12705.

Wu, P.L., Ridley, J., Pardaens, A., Levine, R., Lowe, J., 2015. The reversibility of CO_2 induced climate change. Clim. Dyn. 45, 745–754.

Yoon, J.H., Zeng, N., 2010. An Atlantic influence on Amazon rainfall. Clim. Dyn. 34, 249–264.

Yeh, S.W., Song, S.Y., Allan, R.P., An, S.I., Shin, J., 2021. Contrasting response of hydrological cycle over land and ocean to a changing CO_2 pathway. npj Clim. Atmos. Sci. 4, 53.

Zhang, H., Zhang, M.H., Jin, J.B., Fei, K., Ji, D.Y., Wu, C.L., et al., 2020. Description and climate simulation performance of CAS-ESM version 2. J. Adv. Model. Earth. Syst. 12, e2020MS002210.

Zhang, S.Q., Qu, X., Huang, G., Hu, P., 2023. Asymmetric response of South Asian summer monsoon rainfall in a carbon dioxide removal scenario. npj Clim. Atmos. Sci. 6, 10.

Zhang, S.Q., Qu, X., Huang, G., Hu, P., Zhou, S.J., Wu, L., 2024. Delayed onset of Indian summer monsoon in response to CO_2 removal. Earth. Future 12, e2023EF004039.

Zemp, D.C., Schleussner, C.F., Barbosa, H.M.J., Hirota, M., Montade, V., Sampaio, G., et al., 2017. Self-amplified Amazon forest loss due to vegetation-atmosphere feedbacks. Nat. Commun. 8, 14681.

Zhou, S.J., Huang, P., Xie, S.P., Huang, G., Wang, L., 2022. Varying contributions of fast and slow responses cause asymmetric tropical rainfall change between CO_2 ramp-up and ramp-down. Sci. Bul. 67, 1702–1711.

Ziehn, T., Chamberlain, M.A., Law, R.M., Lenton, A., Bodman, R.W., Dix, M., et al., 2020. The Australian Earth System Model: ACCESS-ESM1.5. J. South. Hemisph. Earth Syst. Sci. 70, 193–214.

Zuo, M., Zhou, T.J., Man, W.M., 2019. Hydroclimate responses over global monsoon regions following volcanic eruptions at different latitudes. J. Clim. 32, 4367–4385.

Please cite this article as: Suqin Zhang, Xia Qu, Gang Huang et al., Reduced rainfall over the Amazon basin in an idealized CO2 removal scenario: Remote dynamic processes, Journal of Environmental Sciences, https://doi.org/10.1016/j.jes.2024.05.035